Front. Earth Sci.
DOI 10.1007/s11707-015-0519-2

RESEARCH ARTICLE

Slope spectrum variation in a simulated loess watershed

Fayuan LI (✉)[1,2], Guoan TANG[1,2], Chun WANG[3], Lingzhou CUI[4], Rui ZHU[5]

1 State Key Laboratory Cultivation Base of Geographical Environment Evolution (Jiangsu Province), Nanjing 210023, China
2 Jiangsu Center for Collaborative Innovation in Geographical Information Resource Development and Application, Nanjing 210023, China
3 Land Information Engineering Department, Chuzhou University, Chuzhou 239000, China
4 College of Life and Environment Science, Wenzhou University, Wenzhou 325035, China
5 Department of Land Surveying and Geo-Informatics, The Hong Kong Polytechnic University, Hong Kong, China

Abstract A simulated loess watershed, where the loess material and relief properly represent the true loess surface, is adopted to investigate the variation in slope spectrum with loess watershed evolution. The evolution of the simulated loess watershed was driven by the exogenetic force of artificial rainfall. For a period of three months, twenty artificial rainfall events with different intensities and durations were carried out. In the process, nine DEM data sets, each with 10 mm grid resolution, were established by the method of close-range photogrammetry. The slope spectra were then extracted from these DEMs. Subsequent series of carefully designed quantitative analyses indicated a strong relationship between the slope spectrum and the evolution of the simulated loess watershed.

Quantitative indices of the slope spectrum varied regularly following the evolution of the simulated loess watershed. Mean slope, slope spectrum information entropy (*H*), terrain driving force (T_d), Mean patch area (*AREA_MN*), Contagion Index (*CONTAG*), and Patch Cohesion Index (*COHESION*) kept increasing following the evolution of the simulated watershed, while skewness (*S*), Perimeter-Area Fractal Dimension (*PAFRAC*), and Interspersion and Juxtaposition Index (*IJI*) represented an opposite trend. All the indices changed actively in the early and active development periods, but slowly in the stable development periods. These experimental results indicate that the time series of slope spectra was able to effectively depict the slope distribution of the simulated loess watershed, thus presenting a potential method for modeling loess landforms.

Keywords slope spectrum, evolution, simulated watershed, loess landform

Received May 4, 2014; accepted January 29, 2015

E-mail: lifayuan@njnu.edu.cn

1 Introduction

Quantification analysis in geomorphology is a key issue in loess landform research in the Loess Plateau of China (Leger, 1990; Feng et al., 2010; Liu et al., 2012). Theory and methodology of digital terrain analysis based on DEMs have been gradually improved (Richard, 2000; Wilson and Gallant, 2000; Florinsky, 2002; Li et al., 2005). Particularly in recent years, critical progress of DEM technology has been achieved and successfully applied to landform research (Maune, 2007; Hengl and Reuter, 2009; Drăguț et al., 2011; Bishop et al., 2012; Evans, 2012; Florinsky, 2012; Wilson, 2012; Bräutigamet al., 2013). Slope spectra, a more integrated terrain index which is not only simple and easy to extract, but also capable of showing the terrain features as well as the development of the loess landform, is proposed (Tang et al., 2008). A slope spectrum is defined as a statistical graph or mathematical model delineating the slope distribution in a certain sample area. The diversification of surface relief and roughness in different loess landform areas diversifies the slope values and its distribution. Therefore, a slope spectrum methodology for loess landform research is proposed in the present study based on the interesting discovery that landform changes can be investigated through a deep and thorough analysis of slope and its distribution. Previous investigations in the Loess Plateau indicated a strong relationship between the slope spectrum and the loess landform types (Tang et al., 2008). A continuous change of slope spectrum from south to north in the northern Shaanxi Loess Plateau area shows an obvious spatial distribution for different loess landforms. Meanwhile, a series of indices of the slope spectrum present a regular pattern of variation following the gradual change of landform type in the Loess Plateau (Li and Tang, 2006; Li, 2007). This truly shows the significance of the slope spectrum method in describing the terrain roughness and landform evolution, which helps to

further understand the landform genesis and spatial distribution rules of different landforms in the Loess Plateau. However, the question remains: will slope spectrum follow a regular pattern of variation following loess landform evolution? How much information about the loess surface we can get through slope spectrum? Therefore, the main purpose of this paper is to get the time series of the slope spectrum and investigate how the slope spectrum will change following the simulated watershed development.

In order to observe long term landform evolution in a short period, an artificial rainfall experiment is an effective method to reveal surface processes. Jin (1995) summarized that the advantages of a simulated experiment are prominent for the reasons that it 1) significantly shortens the temporal and spatial scales, 2) is immune to the time and strength of natural rainfall, 3) has designable boundaries, and 4) makes available the micro-processing of landform evolution and erosion which cannot be observed in field work. Meanwhile, as a basic geomorphologic unit, watersheds are the essential basis of the research on quantification analysis and evolution of loess landforms (Horton, 1932; Lin and Oguchi, 2009; Tang et al., 2009). Therefore, a series of carefully-designed experiments was conducted based on a simulated loess watershed at the Artificial Rainfall Simulation Laboratory of the Institute of Soil and Water Conservation, Chinese Academy of Science. Consequently, a series of slope spectrum indices was found to possess the capacity to comprehensively describe terrain features and the evolutionary stages of the simulated loess watershed.

2 Experiment and data processing

2.1 Artificial rainfall experiment

To create a suitable lab-based simulated watershed in which the loess material and surface relief realistically represent the true surface, a series of statistical analyses based on real loess surfaces and pre-experiments were carried out as a reference (Cui, 2002). Meanwhile, previous research and many suggestions based on experience were considered (Bryan and De Ploey, 1983; Jin, 1995; Lei and Tang, 1995; Borselli et al., 2001). Jing (1995) discussed the effect of slope gradient on soil erosion, which provides a reference for design of the slope of the simulated watershed. Lei and Tang (1995) investigated how we can simulate real rainfall under experimental conditions to the utmost extent. Also, research on the comparability of rainfall, soil, and kinetic energy in the simulation experiment of a soil erosion model proved the feasibility and the reliability of the simulated experiment (Lei et al., 1996; Ben-Hur and Keren, 1997; Xue et al., 2007). The experimental material, Malan loess (Holocene loess, covering the top of the loess stratum), taken from Yanglin County in the southern Loess Plateau, was evenly piled on the test platform. The newly deposited layer was 5 cm thick, and was tamped until the bulk density was 1.39 g/cm^3. The process continued until the total thickness reached around 0.5 m at the outlet, and 2.6 m at the divide. Finally, the loess watershed surface was carefully carved to make the surface and the gully networks similar to the true surface. Table 1 shows the geometric character index of the simulated loess surface. Figure 1 presents the original surface before the artificial rainfall experiment.

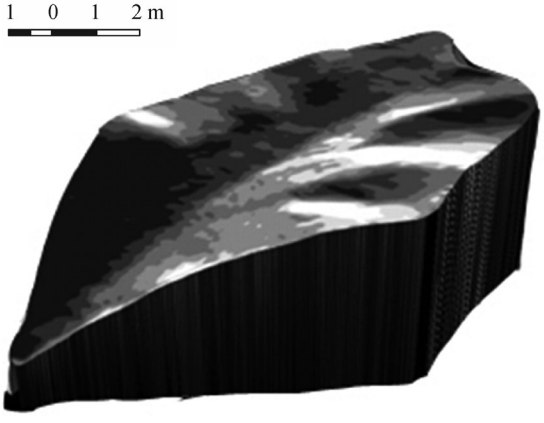

Fig. 1 3D terrain visualization of the initial simulated loess surface.

1) Artificial rainfall: surface erosion was driven by artificial rainfall. The simulated experiment was carried out in the rainfall simulation laboratory for soil erosion processes at the Institute of Soil and Water Conservation, C.A.S. Zhou and Wang (1992), Li et al. (1995), Wang and Jiao (1996) have investigated in detail the rainfall characteristic in the Loess Plateau, which provide us the basis for designing the simulated rainfall process. The rainfall intensity, duration, and interval in the experiment were adjusted to be the same as real rainfall, as far as possible. Duration of the experiment was 72 days, and 2–5 occurrences of rainfall were simulated each week. Table 2 shows all the artificial rainfall parameters in detail.

Table 1 Geometric character indices of the simulated loess surface

Length of watershed/m	Max width /m	Projective area /m^2	Perimeter /m	Elevation difference/m	Longitudinal gradient of watershed/%	Mean slope /(°)	Channel level	Branch ratio
9.1	5.8	31.49	23.3	2.57	28.24	15	2	4

Table 2 Artificial rainfall and close-range photogrammetry parameters

Number of rainfall (sequence of photogrammetry)	Date of rainfall (date of photogrammetry)	Designed rainfall intensity /(mm·h^{-1})	Measured rainfall intensity/(mm·h^{-1})	Duration of rainfall /min	Amount of rainfall /mm
1st stage	(7-29)	Mean: 0.00	Mean: 0.00	Sum: 0.00	Sum: 0.000
1	7-30	30.00	32.4	90.50	48.915
2	8-1	30.00	31.2	89.50	46.540
3	8-3	30.00	29.4	89.50	63.939
4	8-5	60.00	70.8	47.52	65.050
5	8-8	60.00	72.6	45.86	73.580
2nd stage	(8-13)	Mean: 42.00	Mean: 47.4	Sum: 362.88	Sum: 298.024
6	8-14	120.00	144.6	30.53	53.750
7	8-17	60.00	71.4	46.17	51.528
3rd stage	(8-19)	Mean: 90.00	Mean: 108	Sum: 76.80	Sum: 105.278
8	8-20	30.00	34.2	90.18	36.167
9	8-22	30.00	35.4	61.95	55.704
4th stage	(8-27)	Mean: 30.00	Mean: 34.8	Sum: 152.13	Sum: 91.871
10	8-28	60.00	72	47.92	65.360
11	8-31	120.00	129	31.17	65.360
5th stage	(9-1)	Mean: 90	Mean: 106.8	Sum: 79.09	Sum: 130.720
12	9-3	30.00	31.2	62.94	31.896
13	9-5	30.00	34.8	61.53	35.960
14	9-7	30.00	33.6	60.83	34.290
6th stage	(9-11)	Mean: 90	Mean: 33	Sum: 185.30	Sum: 102.146
15	9-11	60.00	67.2	46.82	52.438
16	9-14	60.00	64.8	45.83	49.896
17	9-17	60.00	58.8	47.02	45.256
18	9-20	60.00	62.4	45.37	47.180
7th stage	(9-21)	Mean: 60.00	Mean: 62.4	Sum: 185.04	Sum: 194.770
19	9-24	120.00	127.2	30.37	64.384
20	9-27	120.00	118.8	34.35	67.736
8th stage	(9-28)	Mean: 120.00	Mean: 123	Sum: 64.72	Sum: 132.120
21	9-30	30.00	31.8	91.27	48.373
22	10-9	30.00	33	90.60	49.83
23	10-11	30.00	36	89.72	53.832
9th stage	(10-12)	Mean: 30.00	Mean: 33.6	Sum: 271.59	Sum: 152.035

2) Data collection: close-range photogrammetry was employed in this experiment. The measurement included two procedures: control-survey and close-range photogrammetry. Three datum points were selected as the base of an independent coordinate system and photo-control point surveying. To assure the stability of the whole surveying process, the experiment established three instrument platforms with a forced centering device for the datum points. Meanwhile, there were in total eighteen photo-control points. Twelve of them were laid along the border of the simulated watershed with two-meter intervals, and the remaining six points were set on the ridge of the simulated watershed (Fig. 2). The architecture guaranteed that the number of photo-control points in each image pair was no fewer than six. A two-second high precision electronic theodolite was employed to finish the control survey. A low altitude photography frame of ten meters length, seven meters width, and nine meters height was set up for close-range photogrammetry. SMK-120 stereo camera calibration was set up on the platform to take orthographic photos. DEMs were generated using JX4 digital photogrammetry. Finally, nine sets of DEMs were

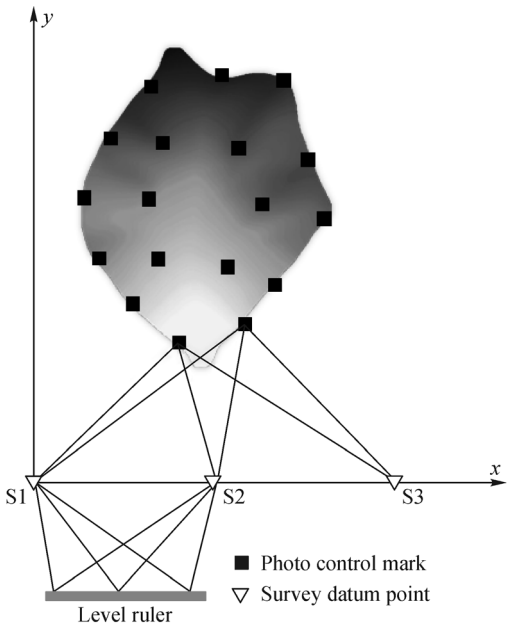

Fig. 2 Control points distribution.

generated at different stages (Fig. 1 and Fig. 3). The grid cell size of the DEM was 10 mm, and the elevation RMSE (Root mean-square error) was less than 2 mm.

2.2 Data preprocessing

Through the experiment of close-range photogrammetry, a set of DEMs at different stages of artificial rainfall were generated, as shown in Table 2. A series of hillshade maps show gradual development of the simulated watershed driven by the artificial rainfall (Fig. 3).

Table 3 Gully density and erosion amount of the simulated watershed

Stage	Gully density/(m·m^{-2})	Erosion amount/kg
I	0.5086	1,355.2
II	0.7404	1,355.2
III	0.865	1,461.3
IV	0.964	1,423.4
V	1.1609	1,881.7
VI	1.3551	979.7
VII	1.847	1,597.7
VIII	2.0437	965.4
IX	1.9488	777.8

The erosion amount could be calculated by subtraction of the two DEMs generated in two consecutive simulation stages (Table 3). The channel networks and gully density of each stage are extracted based on the simulated DEMs

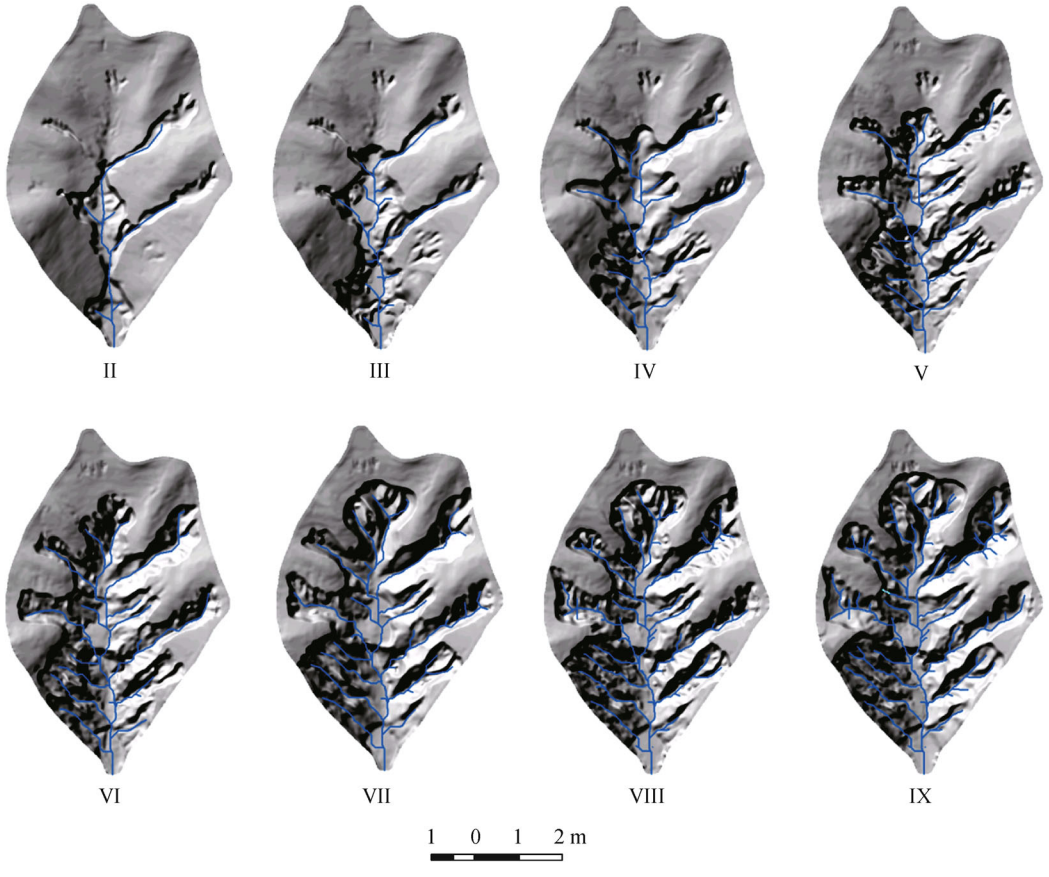

Fig. 3 Hillshade maps of simulated watershed.

(Table 3). Although the gullies did not completely resemble real gullies in shape and scale, they could still represent gullies in real loess landforms to a substantial extent. Slope models at different stages were derived from the DEMs, and the slope spectrum of each stage was established following the method designed by Tang et al. (2008) (Fig. 4 and Fig. 5).

To test the influence of the slope class on slope spectra, we selected DEM of the sixth stage as an example. Stage VI was selected because the watershed is relatively stable and the surface is quite similar to real loess surface. We classified the slope with a slope gradient interval of 1°, 2°, 3°, 4°, 5°, 6°, 10°, 15° and calculated their H (slope spectrum information entropy) and S (skewness). The results show ideal relationships between H, S and slope class (Fig. 6). This means the slope spectra indices will show systematic increase or decrease following the slope gradient interval that we select to establish slope spectra. Hence a comparison analyses is practicable under the same condition of slope class. Tang et al. (2008) suggested that the slope spectra of 3° equal interval class has a more practical applicability in the loess plateau. Therefore, 3° equal interval class is selected as well in the current research.

3 Slope spectrum indices

A histogram-based slope spectrum intuitively delineates the quantity of slope frequencies and can effectively distinguish the relief types and their geomorphologic characteristics of loess landform (Tang et al., 2008). A key step in applying a slope spectrum in digital terrain analysis is to extract a series of quantitative variables by which the morphological significance can be revealed. Based on systematic analyses and comparisons, three factors are selected to quantify the slope spectrum in different aspects. The factors are: 1) the slope spectrum's information entropy (H); 2) the skewness of the slope spectrum (S); and 3) the terrain driving force factor (T_d) (Li and Tang, 2006). Their calculation schemes are based on the following formulas.

3.1 Slope spectrum information entropy

The slope spectrum information entropy is

$$H = -\sum_{i=1}^{m} P_i \ln P_i, \tag{1}$$

where m denotes the number of slope class, and P_i represents the frequency of each slope class. In this research, slope is classified as 3° equal intervals, so that m equals 30. The information entropy of the slope spectrum can appropriately represent the frequency difference of each slope class. For example, in an area of low surface roughness, e.g., the loess table-land region, the distribution of slope mainly ranges from 0−9°, the frequency difference of each slope class is large, and thus, the slope spectrum's information entropy is rather small. In those areas where the surface exhibits high surface roughness, e.g., the loess gully-hill region, the frequency difference of each slope class is lower than that of loess table-land regions, leading to large slope spectrum information entropy (Li, 2007).

3.2 Skewness of slope spectrum

Skewness (S) is used to depict the symmetry of the frequency distribution.

$$s = \frac{m}{(m-1)(m-2)} \sum \left(\frac{p_i - \overline{p}}{\delta} \right)^3, \tag{2}$$

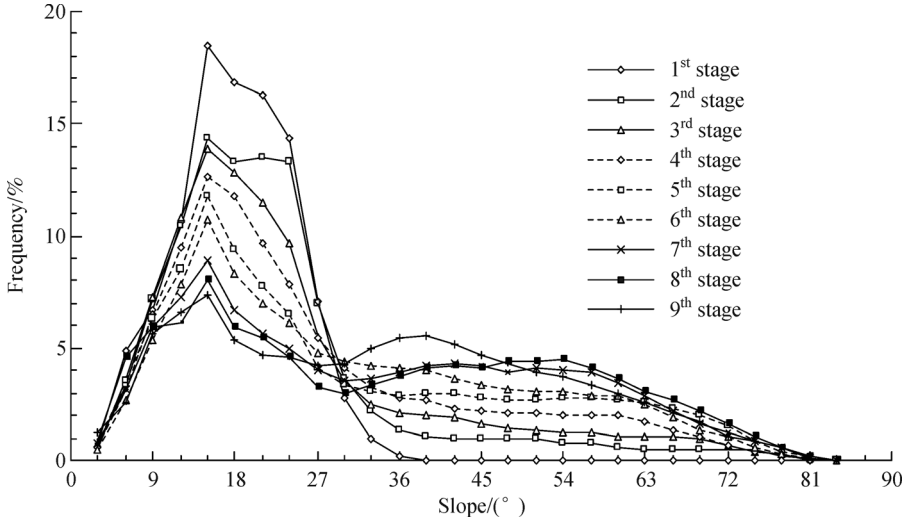

Fig. 4 Slope spectra of simulated watershed in different stages.

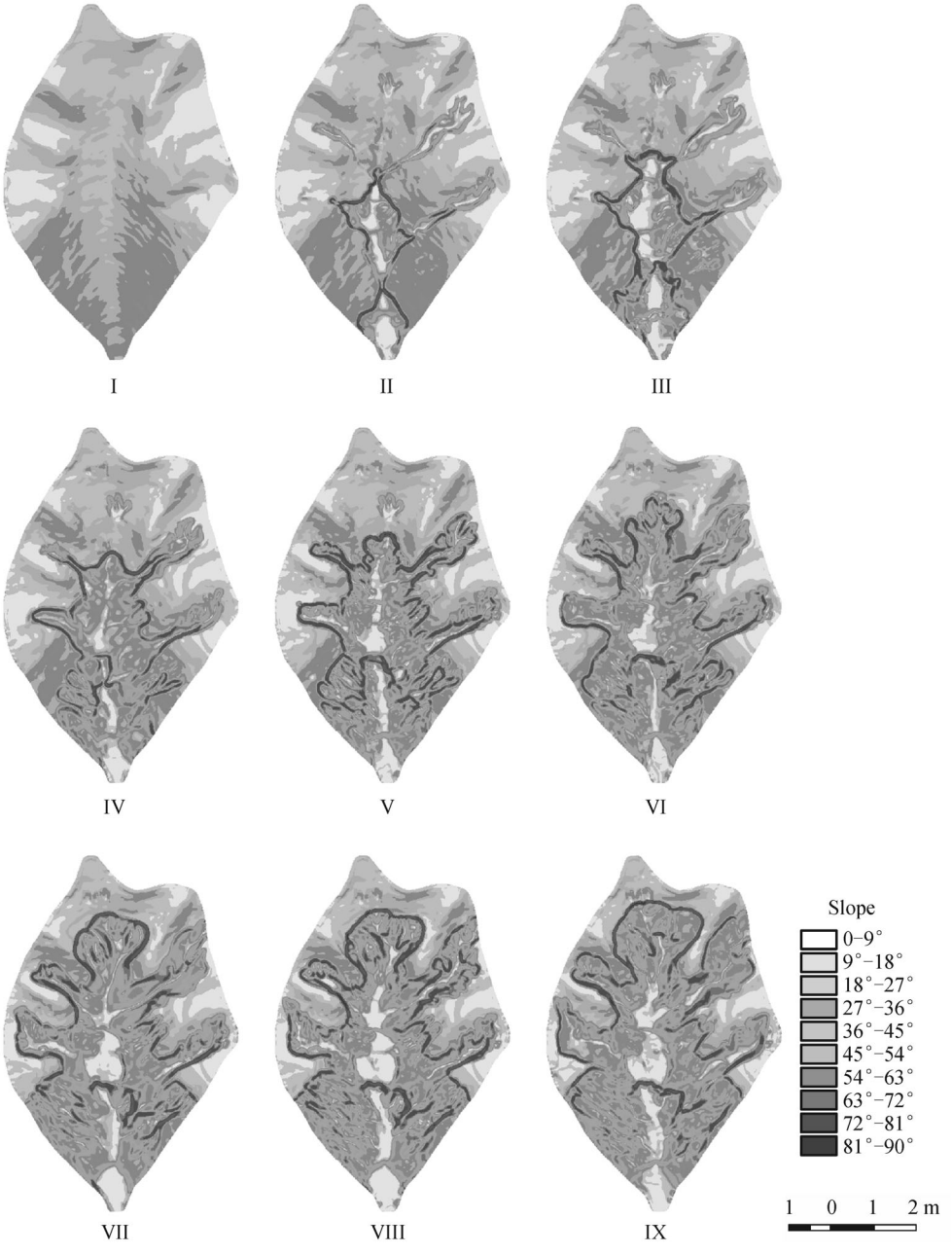

Fig. 5 Slope maps of simulated watershed in different stages.

where m denotes number of slope class, p_i is the frequency of each slope class, $\overline{p}$ is the mean frequency, and δ is the standard deviation.

3.3 Terrain driving force factor

Since any objects on the ground have the potential energy to move downslope because of gravity, to some extent, the sum of energy from a whole watershed could reflect the contribution of the general terrain condition to erosion in the area. The terrain driving force factor (T_d) is represented as:

$$T_d = \frac{\sum_{i=1}^{n}\sum_{j=1}^{m} \sin\ \alpha_{i,j}}{(i \times j)}, \tag{3}$$

where i and j represent the row and column of the grid

DEM respectively, and $\alpha_{i,j}$ is the slope (in degrees) at location *i,j*. The slope gradient is derived from the DEMs, indicating the gradient angle in the direction of maximum slope. In the same conditions (soil property, vegetation covering, etc.), the bigger the T_d is, the stronger the potential energy of downslope movement will be. Hence, T_d is now regarded as a critical regional erosion factor for evaluating erosion level at watershed scale.

Although the three indices (H, T_d, and S) are capable of appropriately depicting the quantitative features of slope frequency distribution, it is difficult to depict the spatial structure of the slope distribution. If each map-patch of slope class can be taken as an independent functional patch, the slope map can be viewed as a landscape unit. Particularly, each map-patch of slope class is the patch of the landscape, all map-patches belonging to the same slope class constitute the class of the landscape, and all the classes constitute an integrated landscape. Then the slope map-patch could be used to depict the patch's spatial structural features, such as relative size, shape, aggregated degree, connectivity degree, etc. Therefore, based on the loess terrain and landscape features, the theory and methodology of landscape ecology could be applied to study the spatial structure of slope distribution. In this paper, five landscape indices are applied to quantify the slope landscape (Table 4).

4 Result and discussion

4.1 Temporal variation of slope spectrum

Figure 4 shows the temporal distribution of the slope spectrum at different stages. Through long term, careful, and thorough observation and analysis, it is found that the average sediment transport ratio at every rainfall stage shows obvious variation during the process of simulated watershed evolution (Fig. 7, Table 5). Based on this, we divided the simulated watershed evolution into three periods, i.e., 1) the early development period (from the 1st rainfall to the 5th rainfall, with DEM stages I–II), 2) the active development period (from the 6th rainfall to the l8th rainfall, with DEM stages III–VI), and 3) the stable development period (from the 19th rainfall to the 25th rainfall, with DEM stages VII–IX). The main erosion types of the watershed are surface erosion and gully headward erosion; the latter includes some gravitational erosion in hill slope areas and deposition at the bottom of the channels. In the early development period, the surface process is dominated by sheet flow erosion, along with downcutting in some depression areas. The slope spectra in this period represent the tendency of the lower gradient to rapidly decrease, and the higher gradient to increase. In the active development period, downcutting in the main branch is extremely active. The gully beds become increasingly undulated with highly developed scarps;

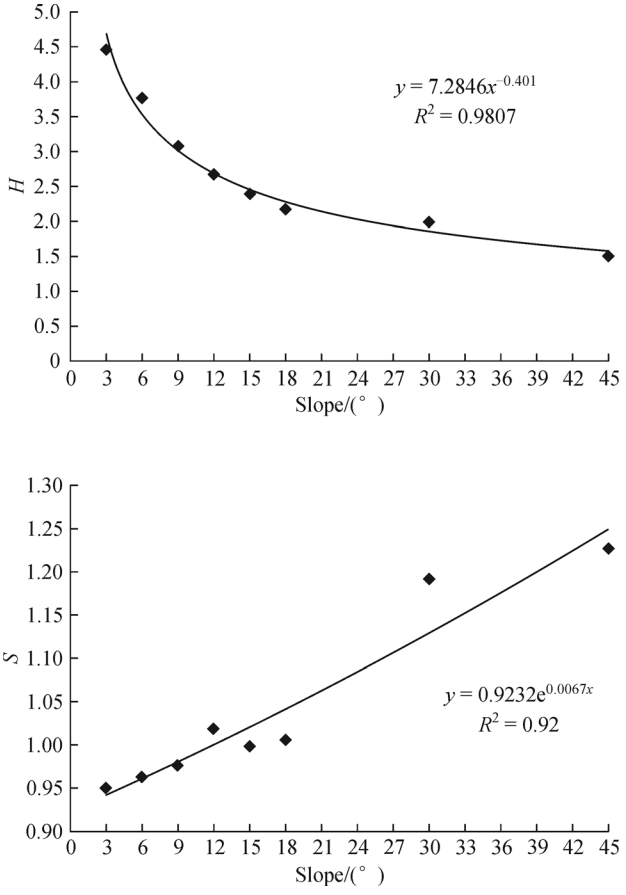

Fig. 6 Variation of H, S with slope class.

meanwhile, accelerated gully headward erosion results in a quick retreat of gully shoulder lines. The slope spectra in this period represent the distribution of the lower gradient gradually shrinking, with the higher gradient rising equivalently. In the stable development period, gully headward erosion is still dominant; however, the retreat of the gully shoulder lines obviously slows down, while gravitational erosion is still active in the hillslope area, in addition to the deposition of upslope eroded materials in some shallow spots. At stages I–VI, the slope distribution shows a trend of increasing to an extreme value quickly, then decreasing. At stages VII–IX the slope spectrum changes slowly, and shows bimodal distribution. An obvious turning point of this set of slope spectra can be found in Fig. 4. Around the gradient of 30°, each slope histogram begins its reversal. It is noticed that there exists an erosion critical slope in the overland flow erosion development between approximately 20 and 30 degrees (Jin, 1995; Hu and Jin, 1999). Whether the figure reveals such an inherent law, is another interesting point waiting to be investigated.

Table 6 shows that at different stages of the simulated watershed, the quantitative indices of the slope spectrum keep changing continuously. The mean slope, slope spectrum information entropy, and terrain driving force

Table 4 Algorithms for the calculation of slope map-patch indices

Quantitative index	Calculation	Remark
Mean patch area (*AREA_MN*)	$AREA\_MN = \sum_{j=1}^{n} \frac{a_{ij}}{n_i}$	a_{ij}: area (m^2) of slope patch ij n_i: patch number reflecting the shape complexity of slope patch
Perimeter-Area Fractal Dimension (*PAFRAC*)	$PAFRAC = \frac{2}{\left[n_i \times \sum_{j=1}^{n} (\ln P_{ij} \times \ln a_{ij})\right] - \left[\left(\sum_{j=1}^{n} \ln P_{ij}\right) \times \left(\sum_{j=1}^{n} \ln a_{ij}\right)\right]}{\left(n_i \times \sum_{j=1}^{n} \ln P_{ij}^2\right) - \left(\sum_{j=1}^{n} \ln P_{ij}\right)^2}$	P_{ij}: perimeter (m) of patch ij n_i: number of patches in the landscape of patch type (class) i comparing the shape complexity of different slope class patch or whole landscape. *PAFRAC* approaches 1 for shapes with very simple perimeters such as squares, and approaches 2 for shapes with highly convoluted, plane-filling perimeters
Contagion Index (*CONTAG*)	$CONTAG = \left[1 + \frac{\sum_{i=1}^{m}\sum_{k=1}^{m}\left[(P_i)\left(\frac{g_{ik}}{\sum_{k=1}^{m} g_{ik}}\right)\right] \times \left(\ln(P_i)\left(\frac{g_{ik}}{\sum_{k=1}^{m} g_{ik}}\right)\right)}{2\ln(m)}\right] \times 100$	P_i: proportion of the landscape occupied by patch type (class) i g_{ik}: number of adjacencies (joins) between pixels of patch types (classes) i and k based on the double-count method. m: number of patch types (classes) present in the landscape, including the landscape border if present. Describing aggregation degree or of slope patch, *CONTAG* approaches 0 when the patch types are maximally disaggregated and interspersed. *CONTAG* = 100 when all patch types are maximally aggregated
Interspersion and Juxtaposition Index (*IJI*)	$IJI = \left[1 + \frac{-\sum_{k=1}^{m}\left[\left(\frac{e_{ik}}{\sum_{k=1}^{m} e_{ik}}\right)\ln\left(\frac{e_{ik}}{\sum_{k=1}^{m} e_{ik}}\right)\right]}{\ln(m-1)}\right] \times 100$	e_{ik}: total length (m) of edge in landscape between patch types (classes) i and k m: number of patch types (classes) *IJI* approaches 0 when the corresponding patch type is adjacent to only 1 other patch type and the number of patch types increases. *IJI* = 100 when the corresponding patch type is equally adjacent to all other patch types
Patch Cohesion Index (*COHESION*)	$COHESION = \left[1 - \frac{\sum_{j=1}^{n} p_{ij}}{\sum_{j=1}^{n} p_{ij}\sqrt{a_{ij}}}\right] \times \left[1 - \frac{1}{\sqrt{A}}\right]^{-1} \times 100$	p_{ij}: perimeter of patch ij a_{ij}: area of patch ij in terms of number of cells A: total number of cells in the landscape describing fragmentation of slope patch or whole landscape $0 \leqslant COHESION \leqslant 100$. *COHESION* at the landscape level is similar to *CONTAG*

Table 5 Sediment transport ratio in different stages (according Cui, 2002)

Stage	Transport amount/kg	Sediment amount/kg	Transport ratio
2nd stage	1,355.2	0	1
3rd stage	1,393.2	68.1	0.953
4th stage	1,302.6	120.8	0.915
5th stage	1,880.6	0.078	0.999
6th stage	912.1	67.6	0.931
7th stage	1,580.8	16.9	0.989
8th stage	946.2	19.2	0.98
9th stage	737.1	40.7	0.948

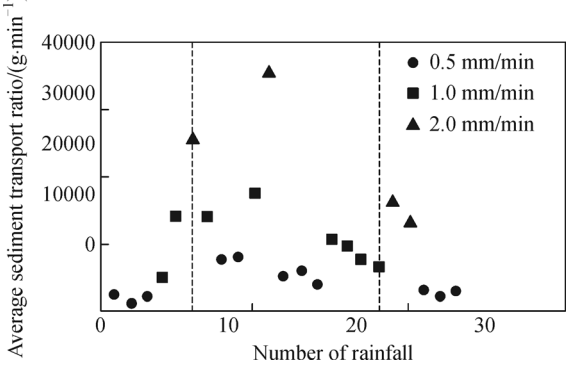

Fig. 7 Scatter map of average sediment transport ratio *vs* rainfall history.

keep increasing with the evolution of the simulated watershed (from stage I–VIII), while their skewness shows an opposite trend. We can notice that in stage IX, the mean slope, slope spectrum information entropy, and terrain driving force decrease a little. The reason is from stage VIII to IX the sediment amount increases a lot (Table 5), which makes the loess surface more smooth.

Table 6 Quantitative indices of slope spectrum in different stages

Stage	Mean slope	Skewness (S)	Slope spectrum information entropy (H)/nat	Terrain driving force (T_d)
I	16.52°	1.563	2.138	0.283
II	20.76°	1.411	2.59	0.342
III	22.73°	1.419	2.755	0.369
IV	25.30°	1.356	2.888	0.406
V	28.79°	1.339	3.033	0.451
VI	29.67°	0.875	3.048	0.468
VII	31.97°	0.313	3.121	0.498
VIII	33.24°	−0.079	3.157	0.514
IX	32.70°	−0.231	3.142	0.511

Gully density is an overall comprehensive geomorphologic index, which can reveal not only the degree of soil erosion, but also the stages of landform evolution (Zhang and Ma, 1998). The gully densities of the simulated watershed are calculated based on the channel networks from the DEMs (Table 3). Correlation analysis of gully density with H and T_d indicates a positive correlation; it increases with H and T_d (Fig. 8(a) and 8(b)). Hence, in the first period, the gully density is still low, as H and T_d values are low. Along with the strengthening of surface erosion, surface roughness also increases. In such circumstances, the H and T_d value have a positive response. In contrast, S and gully density show a negative correlation (Fig. 8(c)), which indicates that the slope distribution has the trend changing to normal distribution with the evolution of simulated watershed, and the surface erosion intensifies gradually as well. These relationships rightly correspond to the finding of research in the loess gully region in northern Shaanxi (Li, 2007). This proves the reliability of the simulated watershed. Therefore, it is likely possible to create a quantitative law for loess landform evolution via slope spectrum analysis. Figures 8(d) and 8(e) reveal a quadratic function relationship of the variation of H and T_d with erosion amount. It illustrates that the variation of slope spectrum was able to yield a close response to surface erosion and sediment.

4.2 Spatial variation of slope spectrum

4.2.1 Indices at class level

Figure 9 shows the distribution of the slope map-patch indices at different stages at class level, which can depict the spatial structure of the patches for different slope classes.

1) Relative size and shape of patches:

AREA_MN of the slope patch was found to have a sudden decrease with continuing rainfall. The peak value of the curve falls in the interval between 0.8 and 3.5 cm^2, which reveals a high sensitivity of original loess surface to irreversible accelerated erosion. Overall, Fig. 9(a) shows that the relative size of the patches is rather small, while the heterogeneity degree is high. *PAFRAC* at different stages varies from 1.17 to 1.83. Following the increase of the slope, *PAFRAC* of the simulated watershed shows the same trend, as does the complexity of the patches. The aforementioned variation of the slope patches indicates that once the rainfall erosion began, the original smooth loess surface became more complicated, i.e., the increasing surface roughness and gully enlargement accelerated headward erosion.

2) Spatial structure of patches:

An *IJI* value approaching 0 indicates that the target patch type is spatially adjacent to only one other patch type, and that the number of patch types increases. An *IJI* value equal to 100 represents spatially adjacent patch types that are equal in length, i.e., the possibility of adjacent patches is equal. *IJI* at slope gradients of 27°–60° are bigger than at other slope classes, showing that slope patches in hillslope areas are more dispersed than in flat areas, e.g., valley areas and interfluve areas. This reveals the phenomenon that gully headward erosion enlarges the degree of fragmentation in the simulated watershed. *COHESION* of all stages varies from 70%–100%. In most stages, the minimum value appears at slope 39°–54° which shows that in high relief areas, the degree of slope patch fragmentation and dispersion are high. This indicates that the continuity of the origin loess surface will change quickly following the watershed evolution driven by rainfall erosion.

4.2.2 Indices at landscape level

Table 7 shows slope patch structure of different stages at landscape level. Five indices show different variation patterns that could be classified into two groups. One group includes *PAFRAC* and *IJI*, which shows rising tendency on a global level following the evolution of the simulated watershed. Another group, including *AREA_MN*, *CONTAG,* and *COHESION*, shows opposite trend with the first group. The *PAFRAC* and *IJI* in the early period are smaller than in the later period, while the *AREA_MN*, *CONTAG,* and *COHESION* in the early period are greater than in the later period. This suggests that, in the early period of simulated watershed, fragmentation of the patches of slope class is rather small, the slope patches distribution is consecutive, and the patch shape is more regular than in the later period. The loess surface in the

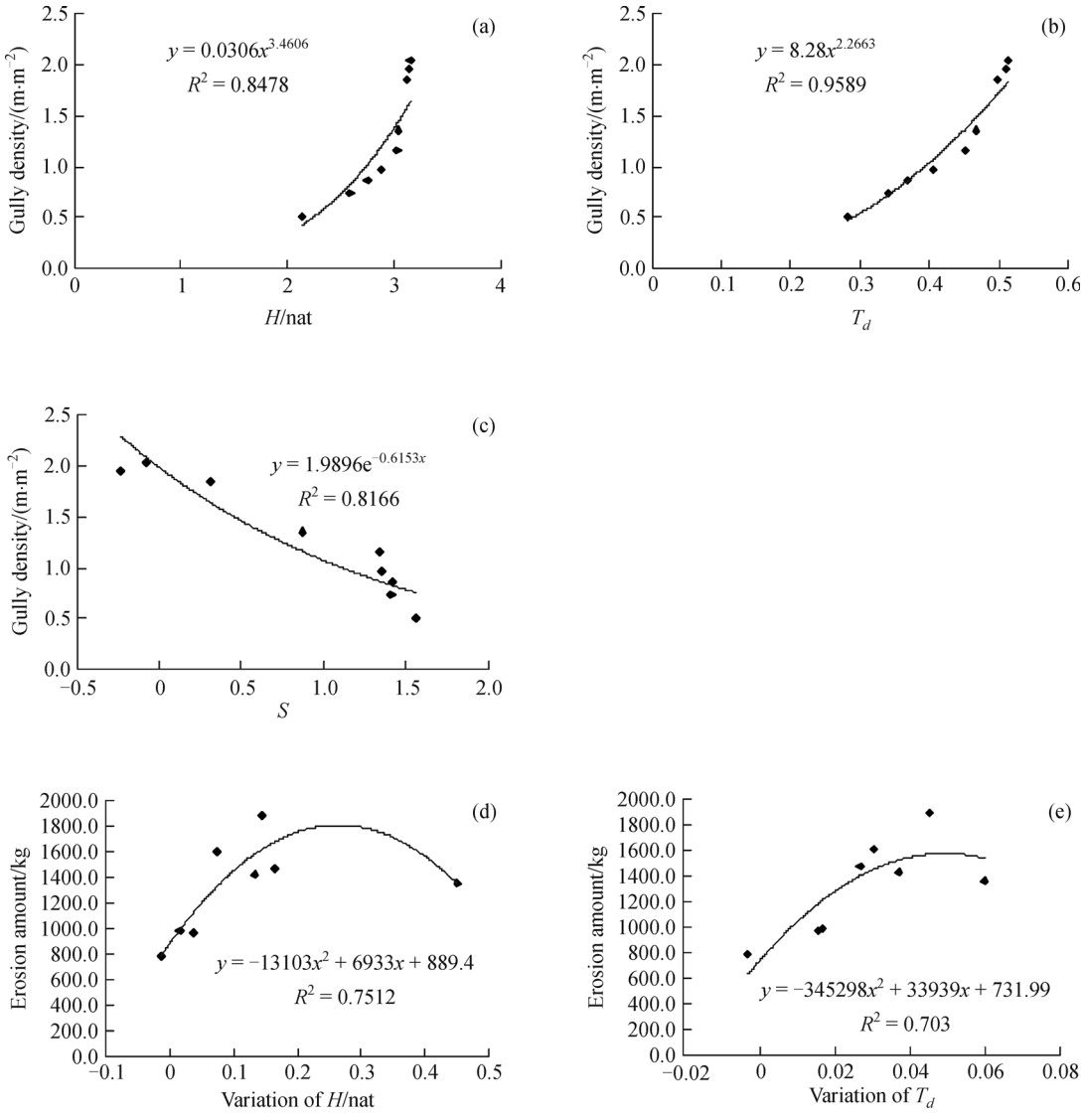

Fig. 8 Comparison of slope spectrum indices with gully density and erosion amount.

early period is smooth, so the *AREA_MN* is larger than in the later stage. This also suggests that, in the early period, fragmentation of slope patches is large, the patches distribute connectively, and the patch shape is more regular than in the later stage. Actually, *PAFRAC* values at different stages show slight difference (ranging from 1.314–1.576), which indicates comparability of the patch shapes in general. This is the same as the indices at class level. All the indices vary following the evolution of the simulated watershed.

5 Conclusions

With the development of geomorphological simulation technology, artificial rainfall experiments are easier to carry out in order to reveal loess surface erosion and landform evolution. To some extent, this experiment presents a basic processing of loess landform development at watershed level.

The time series of the slope spectrum presents an obvious temporal variation following the evolution of the simulated loess watershed. A series of carefully designed indices are capable of reflecting terrain variation of loess watershed. There exists an erosion critical slope approximately 30° in the overland flow erosion development. The *H*, *S*, and T_d show strong relationship with gully density, $R^2 > 0.8$, which means we could use slope spectra indices to demarcate the evolution stage of the simulated watershed. Slope landscape indices in most stages are close to limit value. For instance, the *COHESION* is close to 100, which indicates that the fragmentized degree of the loess surface will increase quickly once the rainfall erosion begins.

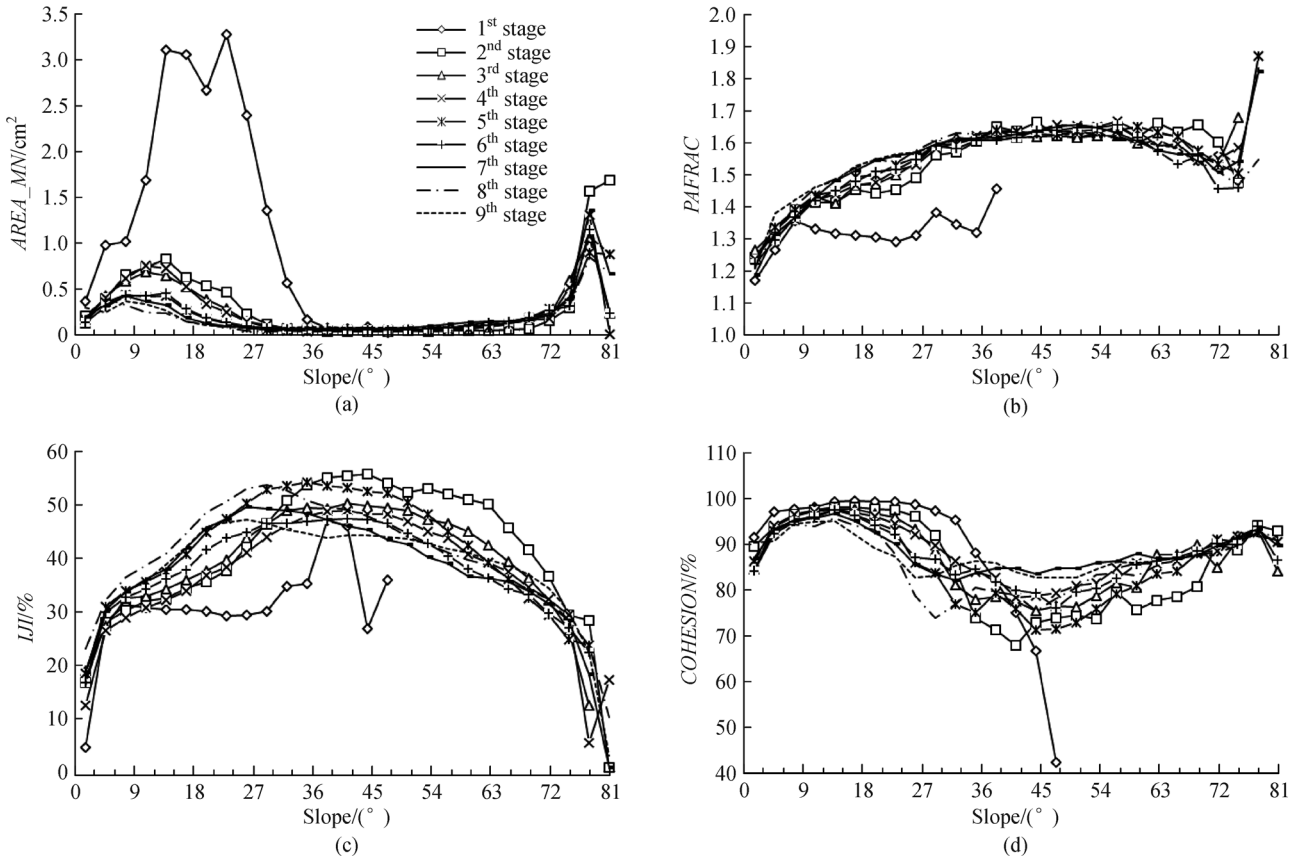

Fig. 9 Comparison of slope map-patch indices' distribution in different stages.

Table 7 Slope map-patch indices in different stages at landscape level

Stage	*AREA_MN* /m^2	*PAFRAC*	*CONTAG*/%	*IJI*/%	*COHESION* /%
I	1.982	1.314	55.217	48.958	99.08
II	0.218	1.512	49.865	62.631	95.992
III	0.184	1.538	45.676	63.638	94.438
IV	0.166	1.555	42.402	63.37	93.36
V	0.103	1.569	37.325	67.155	90.728
VI	0.121	1.565	37.324	64.355	90.655
VII	0.116	1.577	35.598	64.979	89.97
VIII	0.091	1.579	34.26	65.91	87.47
IX	0.109	1.576	34.22	64.749	88.197

The slope spectrum is potentially capable of delineating the spatial or temporal distribution of surface slope in a simulated watershed. As an extension of the concept and methodology of slope spectra, slope landscape is proved to be capable of effectively depicting the spatial structure of slope distribution and other rules of slope variation during the simulated watershed development. A continuous change of slope spectrum shows a strong relationship between slope spectrum and simulated watershed.

In the simulated watershed, the incisions reached the border of the simulated watershed from the 5th stage. This rarely happens in reality, as the concrete border restricts the enlargement of the watershed at the expenses of its neighbor. This limitation of the simulation reduces the reliability of the simulated model to some extent.

Further work should focus on detailed field monitoring of the development of real loess surface driving by field artificial rainfall. Only in this way will it be possible to maintain the original soil structure, an essential factor of soil properties, so as to ensure the validity of the simulated experiment to the utmost extent. Further research can also focus on the connection between micro-lab simulations and macro reality research, as well as between digital terrain analysis and landscape ecology analysis, which is beneficial to promote quantitative research on surface process modeling.

Acknowledgements We are grateful for the financial support from the National Natural Science Foundation of China (Grant Nos. 41171299 and 41271438), the Priority Academic Program Development of Jiangsu Higher Education Institutions (164320H116) and the foundation of State Key Laboratory of Soil Erosion and Dryland Farming on the Loess Plateau (10501-1217, K318009902-13). We are also grateful to Dr. Josef Strobl for his constructive critique of the manuscript. The constructive criticisms and suggestions from anonymous reviewers are also gratefully acknowledged.

References

Ben-Hur M, Keren R (1997). Polymer effects on water infiltration and soil aggregation. Soil Science Society of America Journal, 61(2): 565–570

Bishop M P, James L A, Shroder Jr J F, Walsh S J (2012). Geospatial technologies and digital geomorphological mapping: concepts, issues and research. Geomorphology, 137(1): 5–26

Borselli L, Torri D, Poesen J, Sanchis P S (2001). Effects of water quality on infiltration, runoff and interrill erosion processes during simulated rainfall. Earth Surf Process Landform, 26: 329–342

Bräutigam B, Zink M, Hajnsek I, Krieger G (2013). The TanDEM-X mission: earth observation in 3D. In: Proceeding of Geomorphometry 2013, http://www.geomorphometry.org/Braeutigam2013

Bryan R B, De Ploey J (1983). Comparability of soil erosion measurements with different laboratory rainfall simulators. In: de Ploey, ed. Rainfall Simulation, Runoff and Soil Erosion. Catena Supplement 4, Catena verlag, Cremlingen, WG: 33–56

Cui L Z (2002). The Coupling Relationship between the Sediment Yield from Rainfall Erosion and the Topographic Feature of the Watershed. Dissertation for PhD degree. Yanling: Northwest Agriculture & Forest University (in Chinese)

Drăguț L, Eisank C, Strasser T (2011). Local variance for multi-scale analysis in geomorphometry. Geomorphology, 130(3–4): 162–172

Evans I S (2012). Geomorphometry and landform mapping: what is a landform? Geomorphology, 137(1): 94–106

Feng X M, Wang Y F, Chen L D, Fu B J, Bai G S (2010). Modeling soil erosion and its response to land-use change in hilly catchments of the Chinese Loess Plateau. Geomorphology, 118(3–4): 239–248

Florinsky I V (2002). Errors of signal processing in digital terrain modeling. International Journal of Geographical Information Science, 16(5): 475–501

Florinsky I V (2012). Digital Terrain Analysis in Soil Science and Geology. San Diego: Elsevier Academic Press

Hengl T, Reuter I H (2009). Geomorphometry: Concepts, Software, Application. Amsterdam: Elsevier press

Horton R E (1932). Drainage basin characteristics. Trans Am Geophys Union, 13(1): 350–361

Hu S X, Jin C X (1999). Theoretical analysis and experimental study on the critical slope of erosion. Acta Geographica Sinica, 54(4): 347–356 (in Chinese)

Jin D S (1995). Experiments and Simulations in Geomorphology. Beijing: Earthquake press (in Chinese)

Jing C X (1995). A theoretical study on critical erosion slope gradient. Acta Geographica Sinica, 50(3): 234–239 (in Chinese)

Leger M (1990). Loess landforms. Quat Int, 7–8: 53–61

Lei A L, Shi Y X, Tang K L (1996). Soil comparability in the simulation experiment of soil erosion model. Chin Sci Bull, 41(19): 1801–1804 (in Chinese)

Lei A L, Tang K L (1995). Rainfall comparability and realization in the simulation experiment of soil erosion model. Chin Sci Bull, 40(21): 2004–2006 (in Chinese)

Li C X, Shen J, Fan R S (1995). Characteristic analysis of rainfall spatial variability on small catchments in loess regions. Advances in Water Science, 6(2): 12–16 (in Chinese)

Li F Y (2007). Research on the Slope Spectrum and Its Spatial Distribution in the Loess Plateau. Dissertation for PhD degree. The Graduate University of Chinese Academy of Sciences, Beijing (in Chinese)

Li F Y, Tang G A (2006). DEM based research on the terrain driving force of soil erosion in the Loess Plateau. In: Gong J A, Zhang J X, eds. Proceedings of Geoinformatics 2006: Geospatial Information Science, 6420: 64201W1-8

Li Z L, Zhu Q, Gold C M (2005). Digital Terrain Modeling: Principles and Methodology. New York: CRC Press

Lin Z, Oguchi T (2009). Longitudinal and transverse profiles of hilly and mountainous watersheds in Japan. Geomorphology, 111(1–2): 17–26

Liu G, Xu W N, Liu P L, Yang M Y, Cai C F, Zhang Q (2012). Slope development of tableland in the Holocene on the Chinese Loess Plateau. J Food Agric Environ, 10(2): 1164–1167

Maune D F (2007). Digital Elevation Model Technologies and Applications: The Dem Users Manual (2nd ed). American Society for Photogrammetry and Remote Sensing Publisher

Richard J P (2000). Geomorphometry– diversity in quantitative surface analysis. Progress in Physical Geography, 24(1): 1–30

Tang G A, Jia Y N, Qumu W Z (2009). The terrain analysis based on profile line of catchment boundary of loess landform. International Postgraduate Conference on Infrastructure and Environment, 2009, Hongkong, China

Tang G A, Li F Y, Liu X J, LongY, Yang X (2008). Research on the Slope Spectrum of the Loess Plateau. Science China Series E, 51(S1): 175–185

Wang W Z, Jiao J Y (1996). Rainfall Erosion in the Loess Plateau and the Yellow River Sediment. Beijing: Science China Press (in Chinese)

Wilson J P (2012). Digital terrain modeling. Geomorphology, 137(1): 107–121

Wilson J P, Gallant J C (2000). Terrain Analysis: Principles and Applications. New York: John Wiley & Sons

Xue Y N, Xu X Z, Wang R R, Chen F (2007). Principle and method to simulate rainfall with the similar kinetic energy. Science of Soil and Water Conservation, 5(6): 102–105 (in Chinese)

Zhang L P, Ma Z Z (1998). The research on the relation between gully density and cutting depth in different drainage landform evolution periods. Geographical research, 17(3): 273–278 (in Chinese)

Zhou P H, Wang Z L (1992). A study on rain storm causing soil erosion in the Loess Plateau. J Soil Water Conserv, 6(3): 1–5 (in Chinese)